Supplemental Material

Journal of Hydrometeorology

Improved Snow Albedo Evolution in Noah-MP Land Surface Model Coupled with a Physical Snowpack Radiative Transfer Scheme

https://doi.org/10.1175/JHM-D-24-0082.1

Supplemental Material

Improved snow albedo evolution in Noah-MP land surface model coupled with a physical snowpack radiative transfer scheme

Tzu-Shun Lin,[a] Cenlin He,[a] Ronnie Abolafia-Rosenzweig,[a] Fei Chen,[b] Wenli Wang,[c] Michael Barlage,[d] and David Gochis[e]

[a] *NSF National Center for Atmospheric Research, Boulder, CO, USA*

[b] *Hong Kong University of Science and Technology, Hong Kong, China*

[c] *Institute of Atmospheric Physics, Chinese Academy of Sciences, Beijing, China*

[d] *NOAA/Environmental Modeling Center, College Park, MD, USA*

[e] *Airborne Snow Observatories, Inc., Crowley Lake, CA, USA*

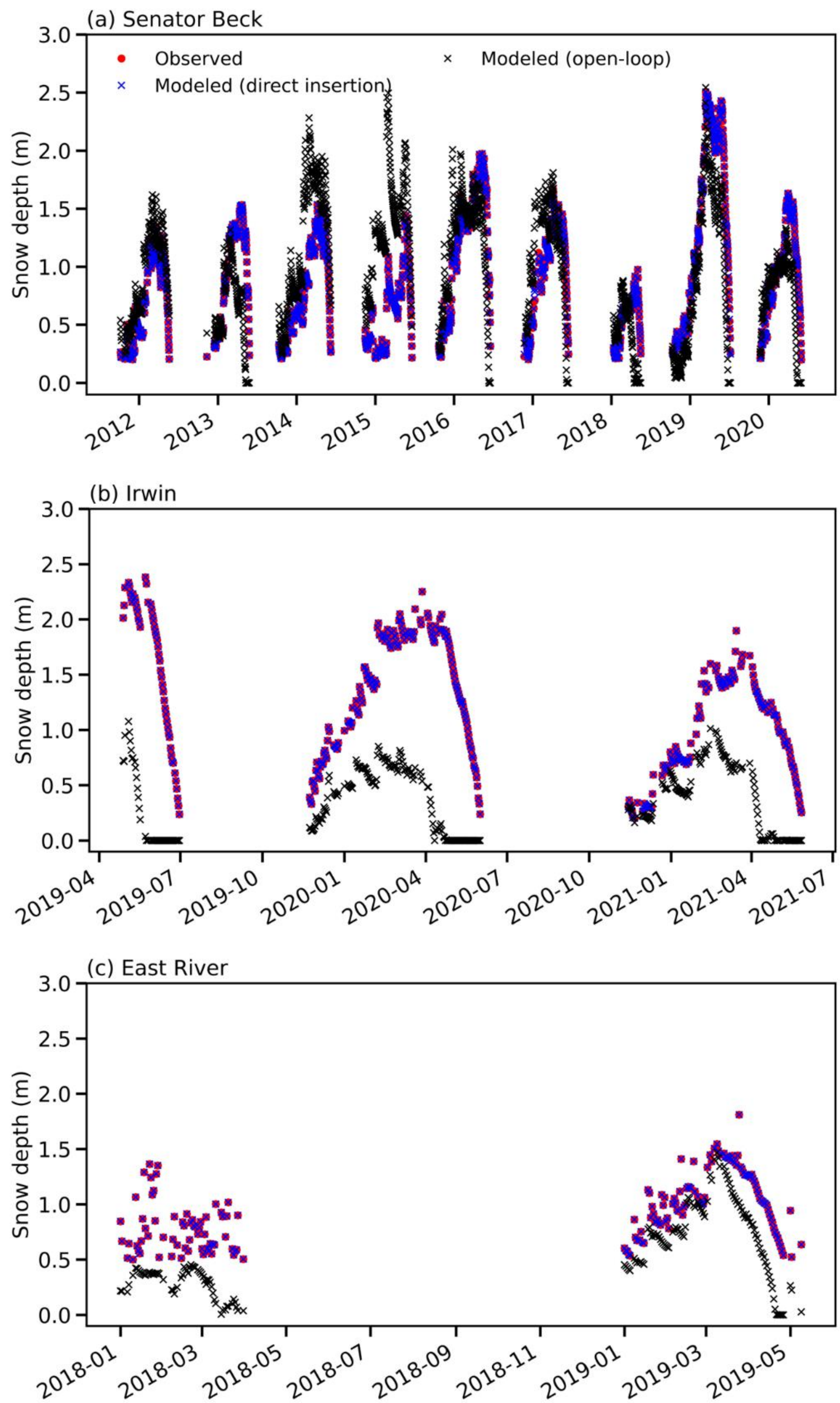

Fig. S1. The comparison of the observed (red circles) and Noah-MP simulated snow depth from direct insertion (blue cross markers) and open-loop run (black cross markers) at three stations, (a) Senator Beck, (b) Irwin, and (c) East River.

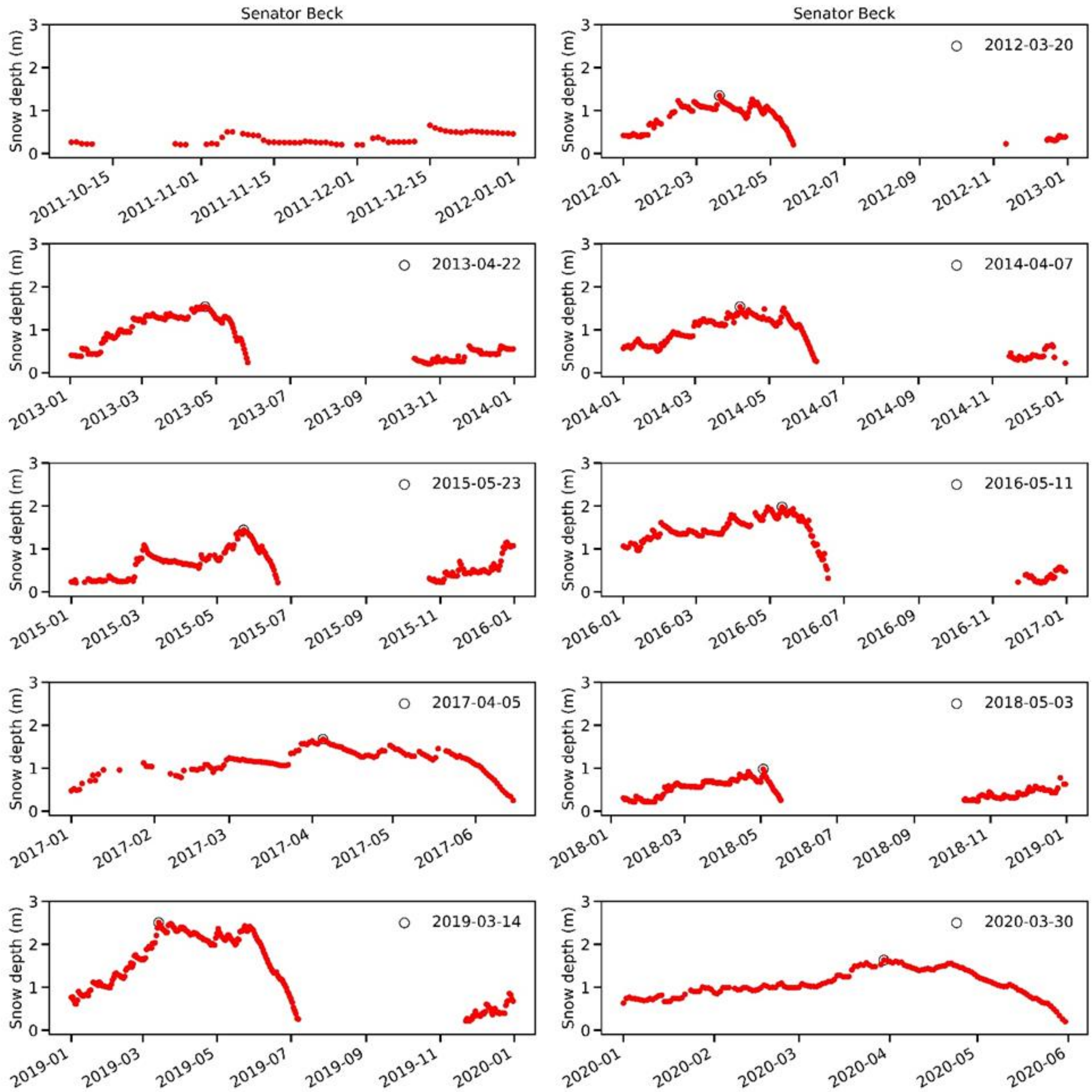

Fig. S2a. Observed snow depth with time (red dots) and the date for annual peak snow depth (black circle) at the Senator Beck site.

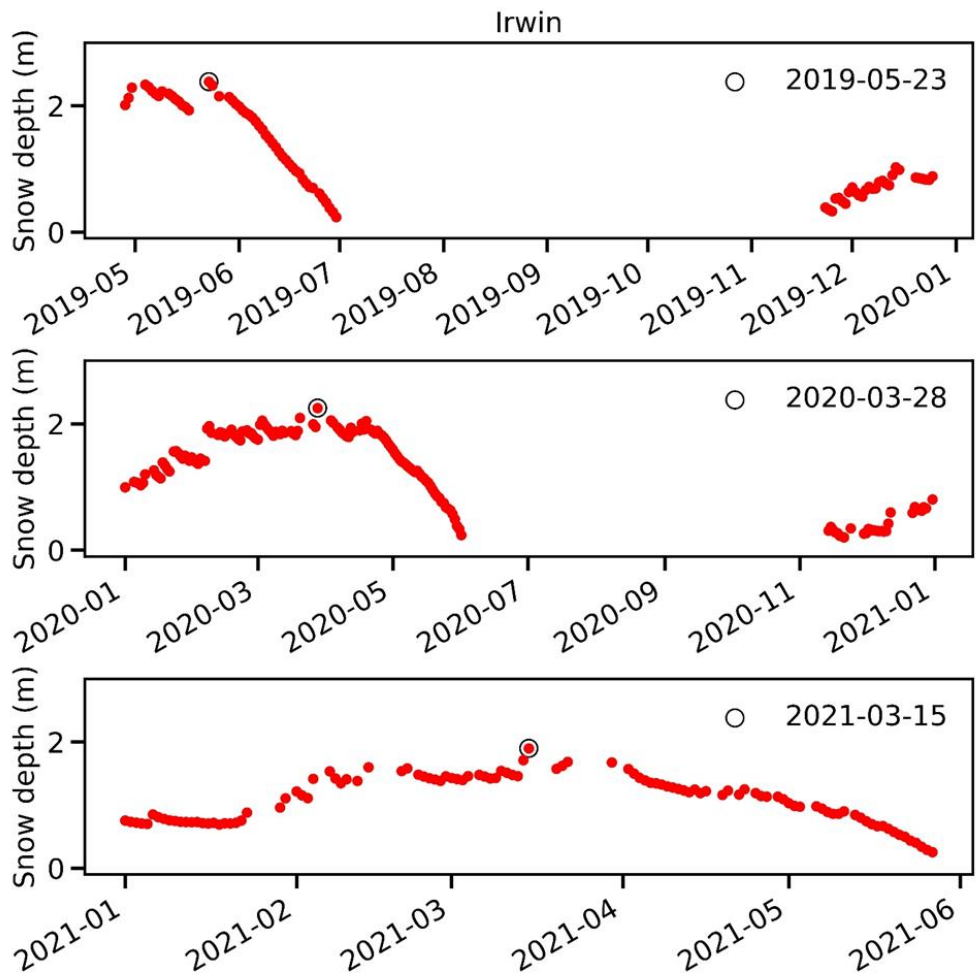

Fig. S2b. Similar to Fig. S2a but at the Irwin site.

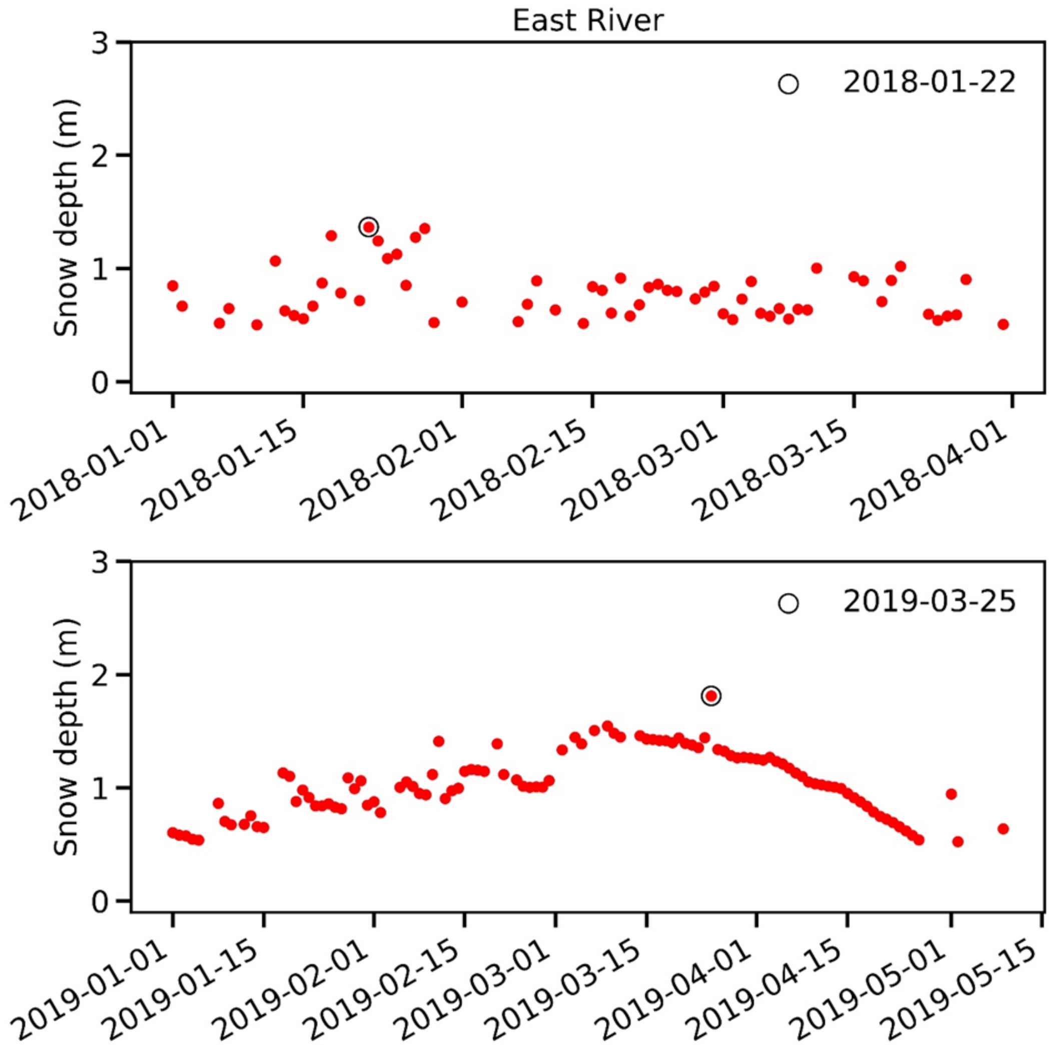

Fig. S2c. Similar to Fig. S2a but at the East River site.

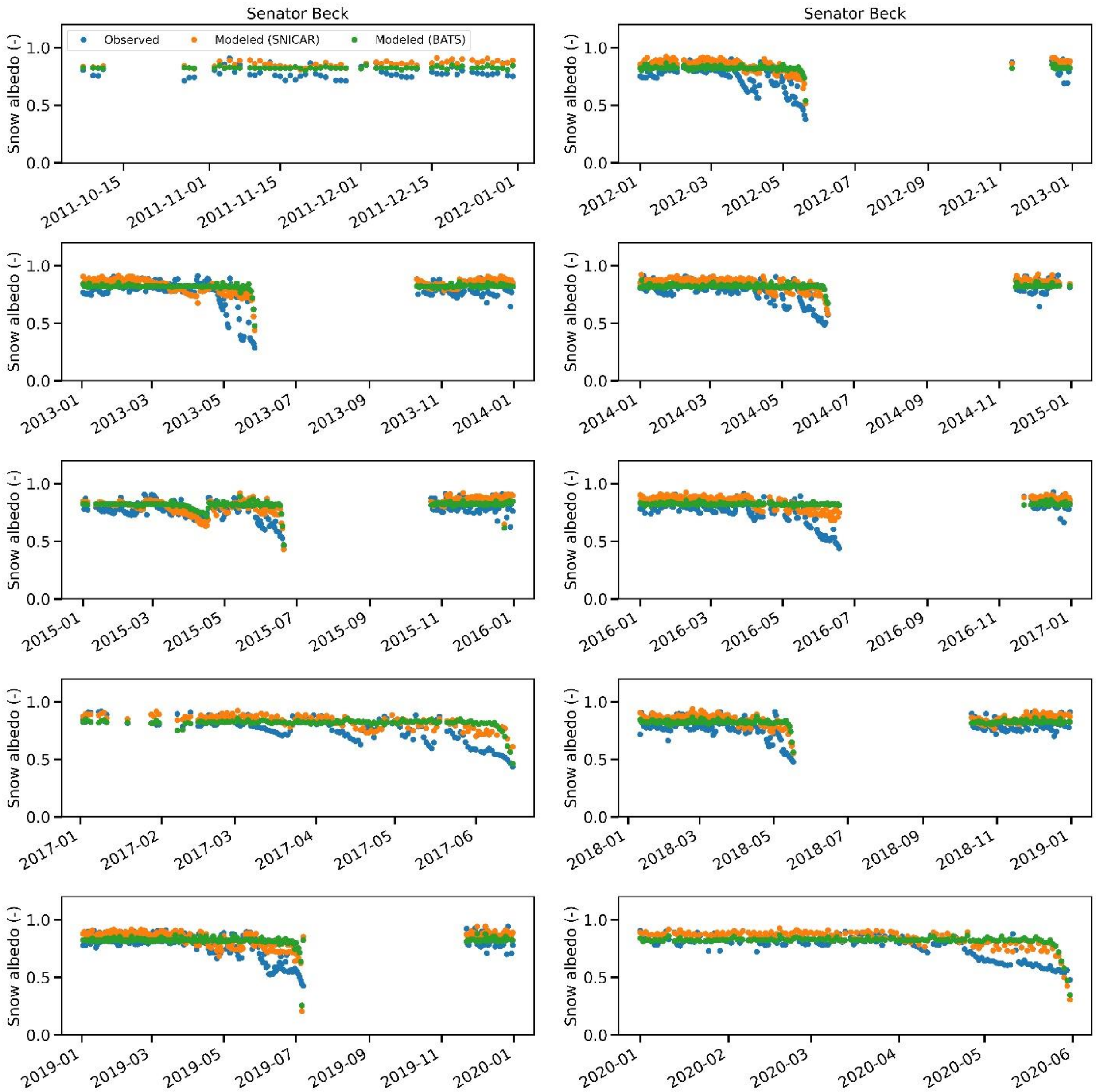

Fig. S3a. The comparison of observed (blue dots), NoahMP-BATS (orange dots), and NoahMP-SNICAR (green dots) simulated snow albedo in broadband at the Senator Beck site.

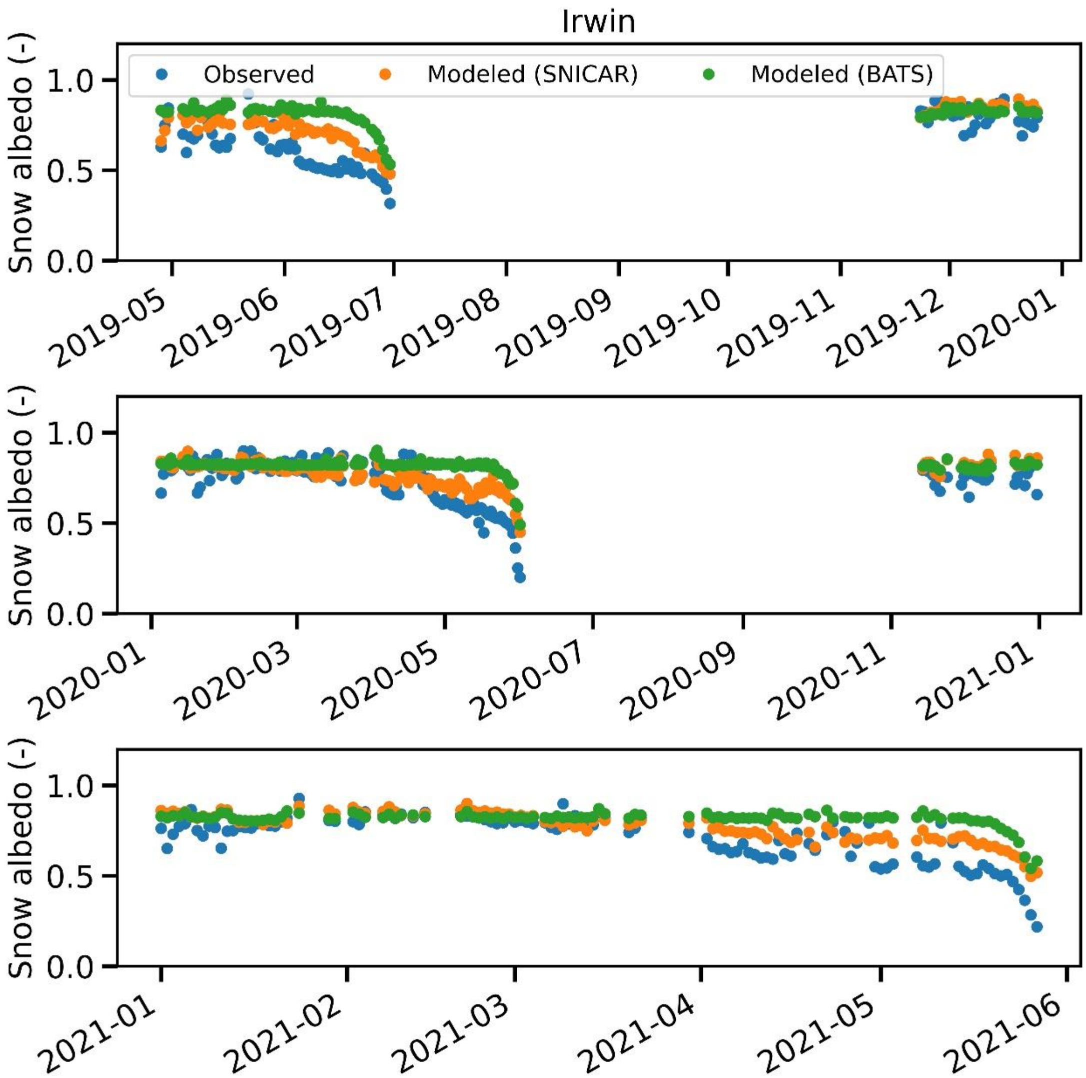

Fig. S3b. Similar to Fig. S3a but at the Irwin site.

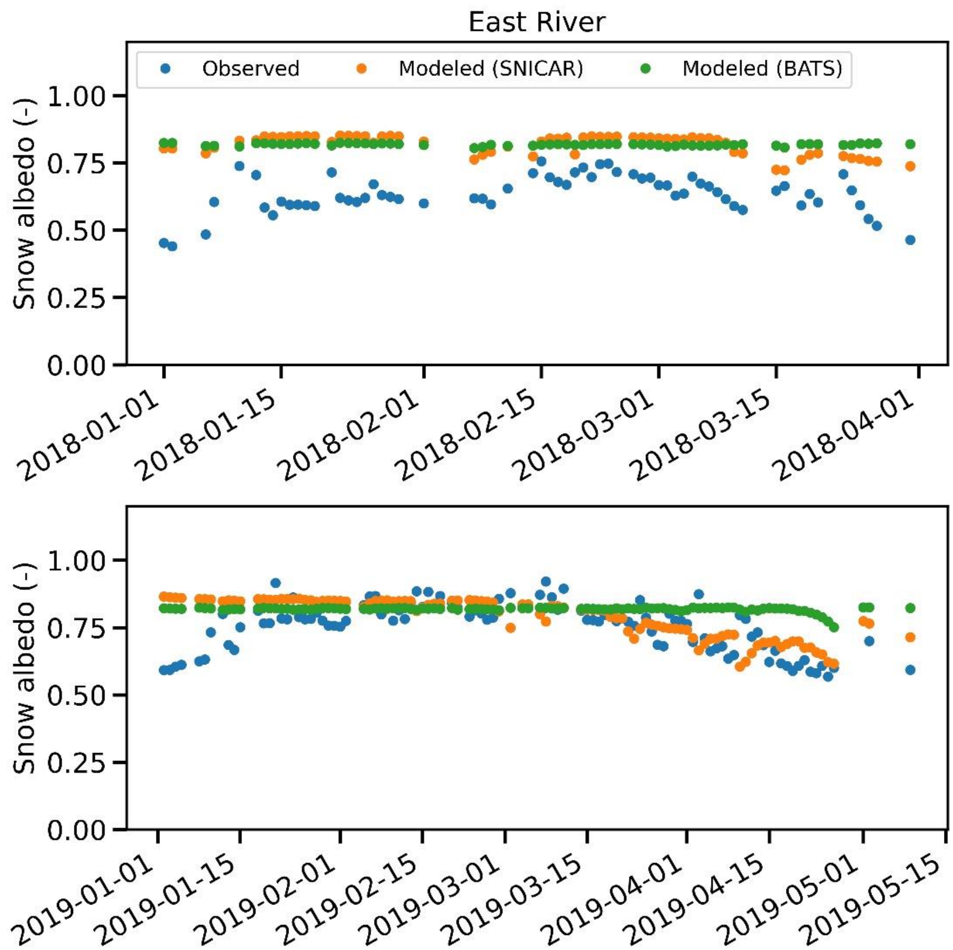

Fig. S3c. Similar to Fig. S3a but at the East River site.

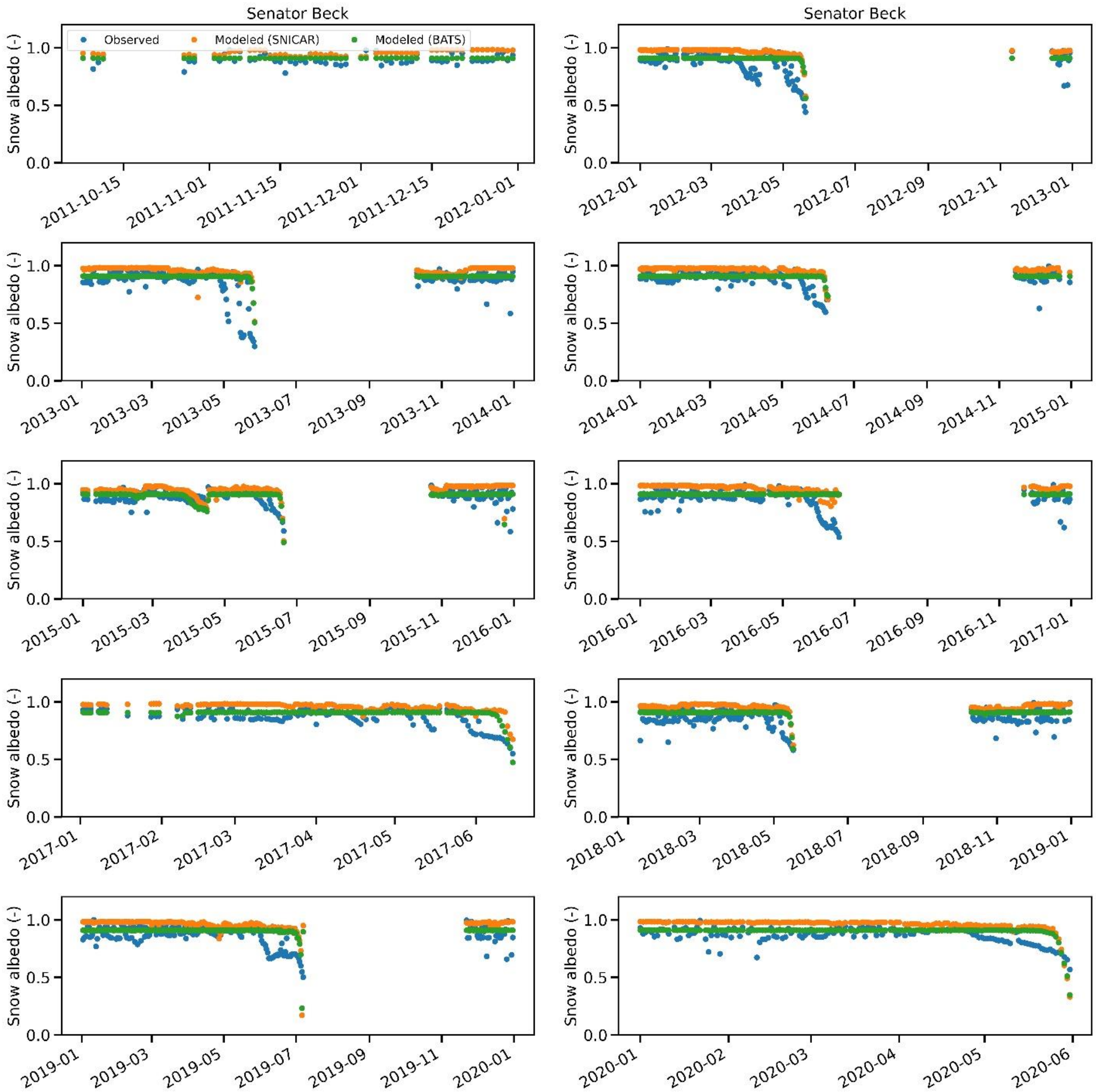

Fig. S4a. Similar to Fig. S3a but in visible wavelengths.

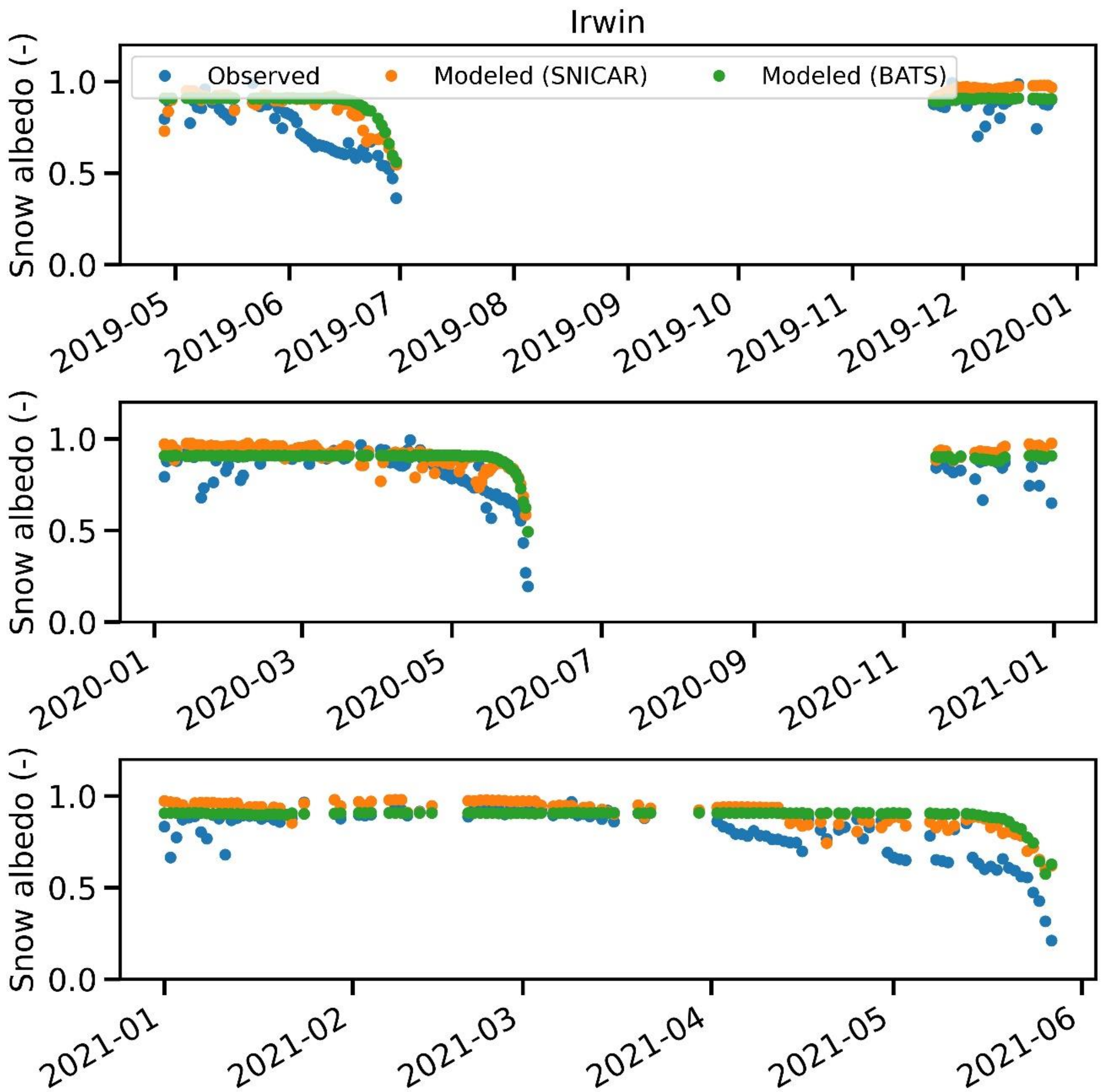

Fig. S4b. Similar to Fig. S3b but in visible wavelengths.

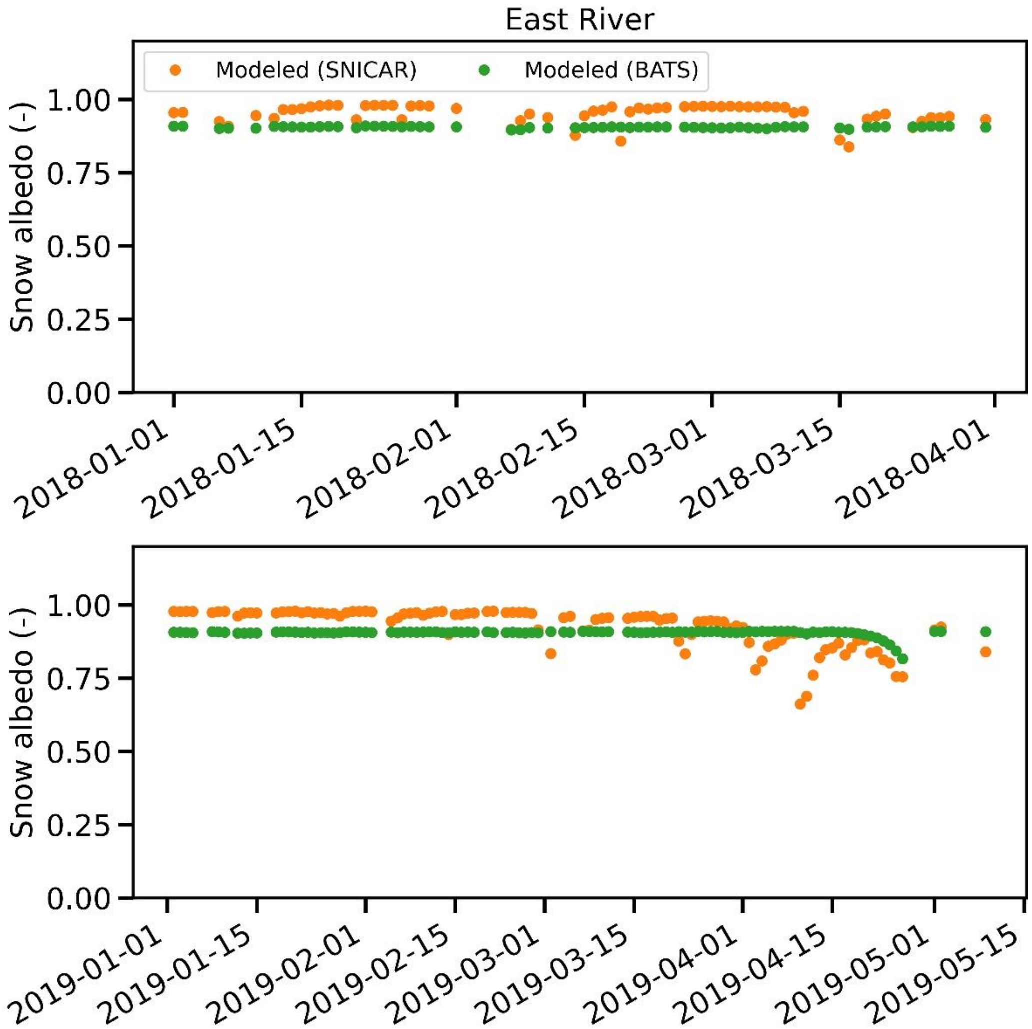

Fig. S4c. Similar to Fig. S3c but in visible wavelengths.

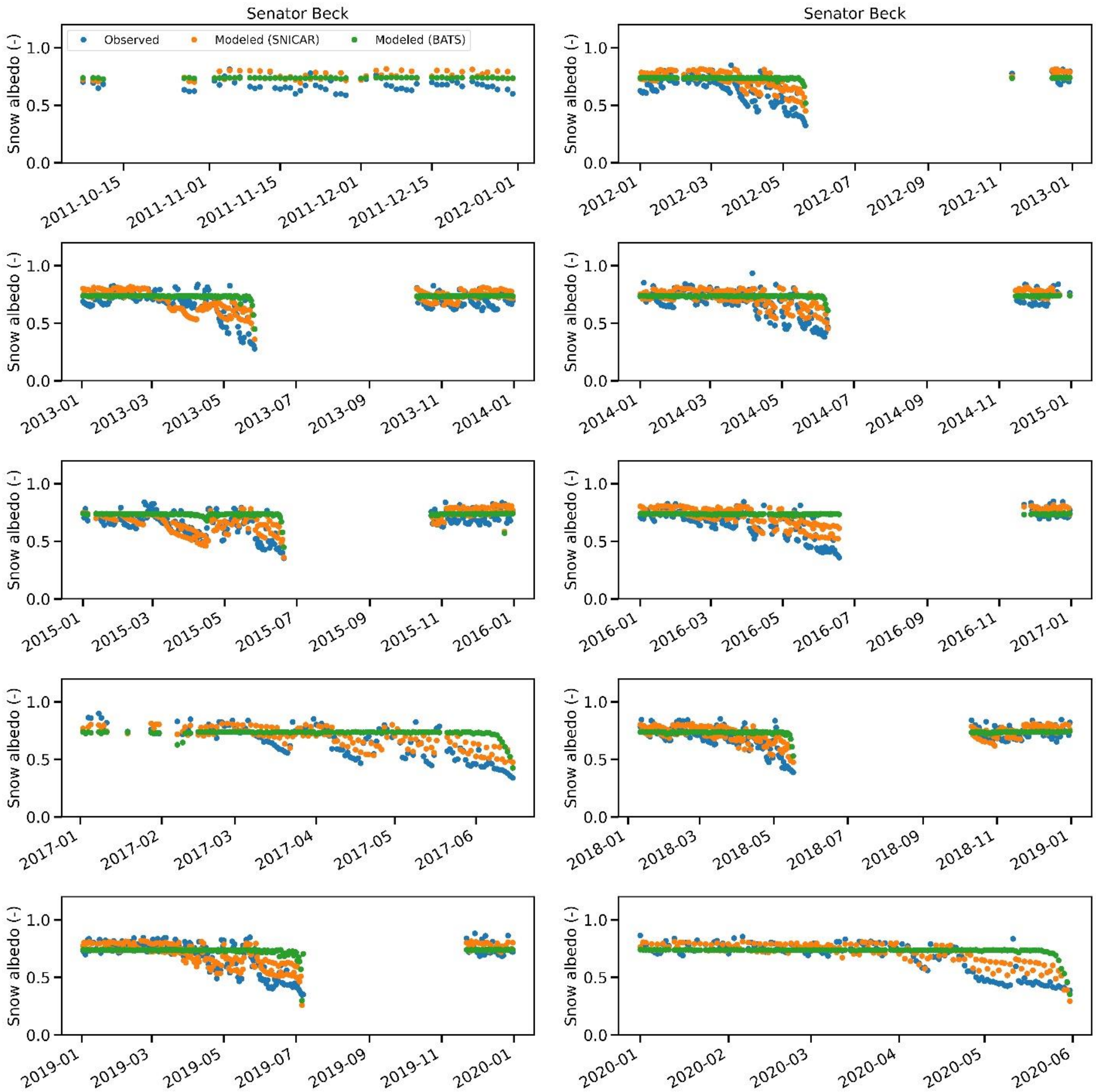

Fig. S5a. Similar to Fig. S3a but in near-infrared wavelengths.

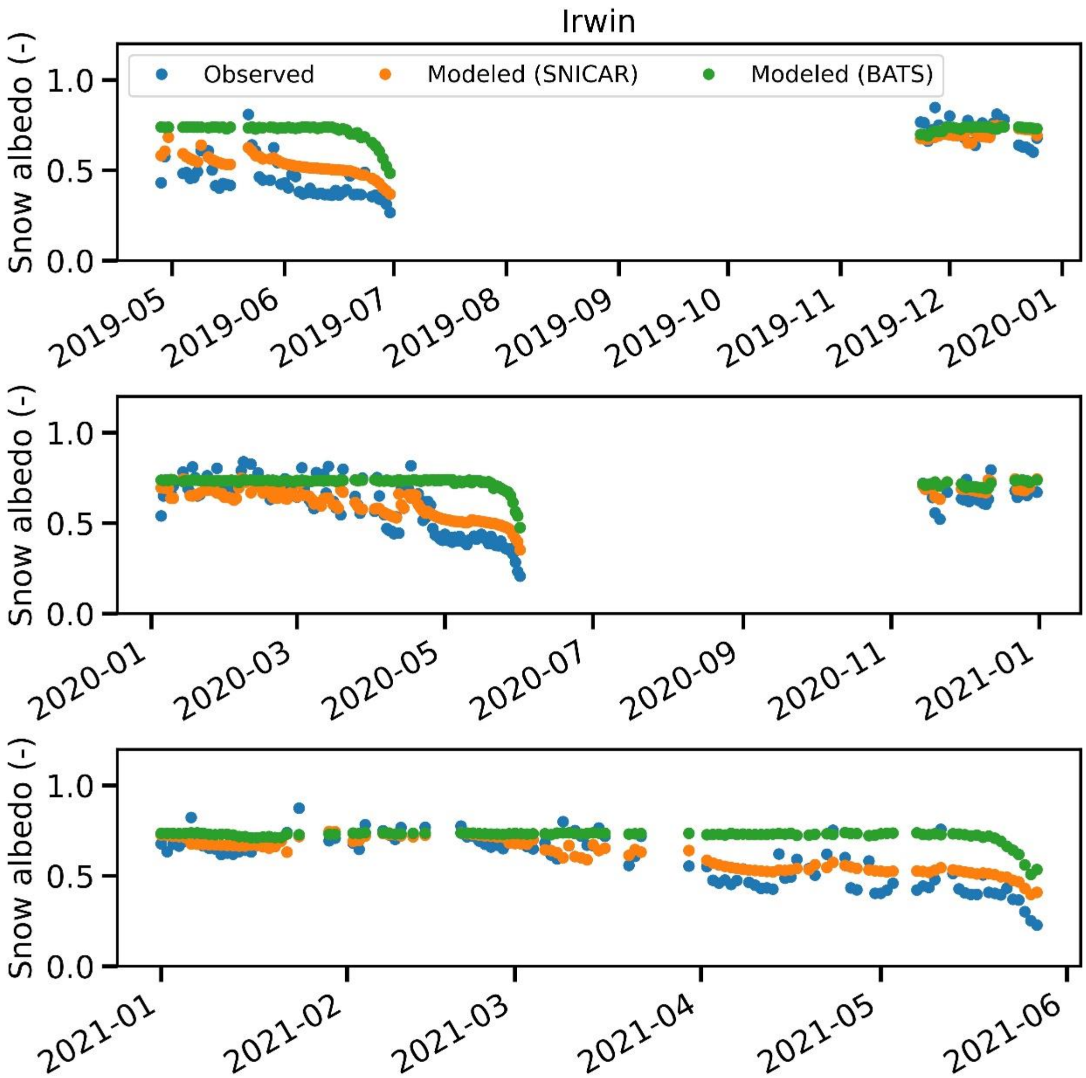

Fig. S5b. Similar to Fig. S3b but in near-infrared wavelengths.

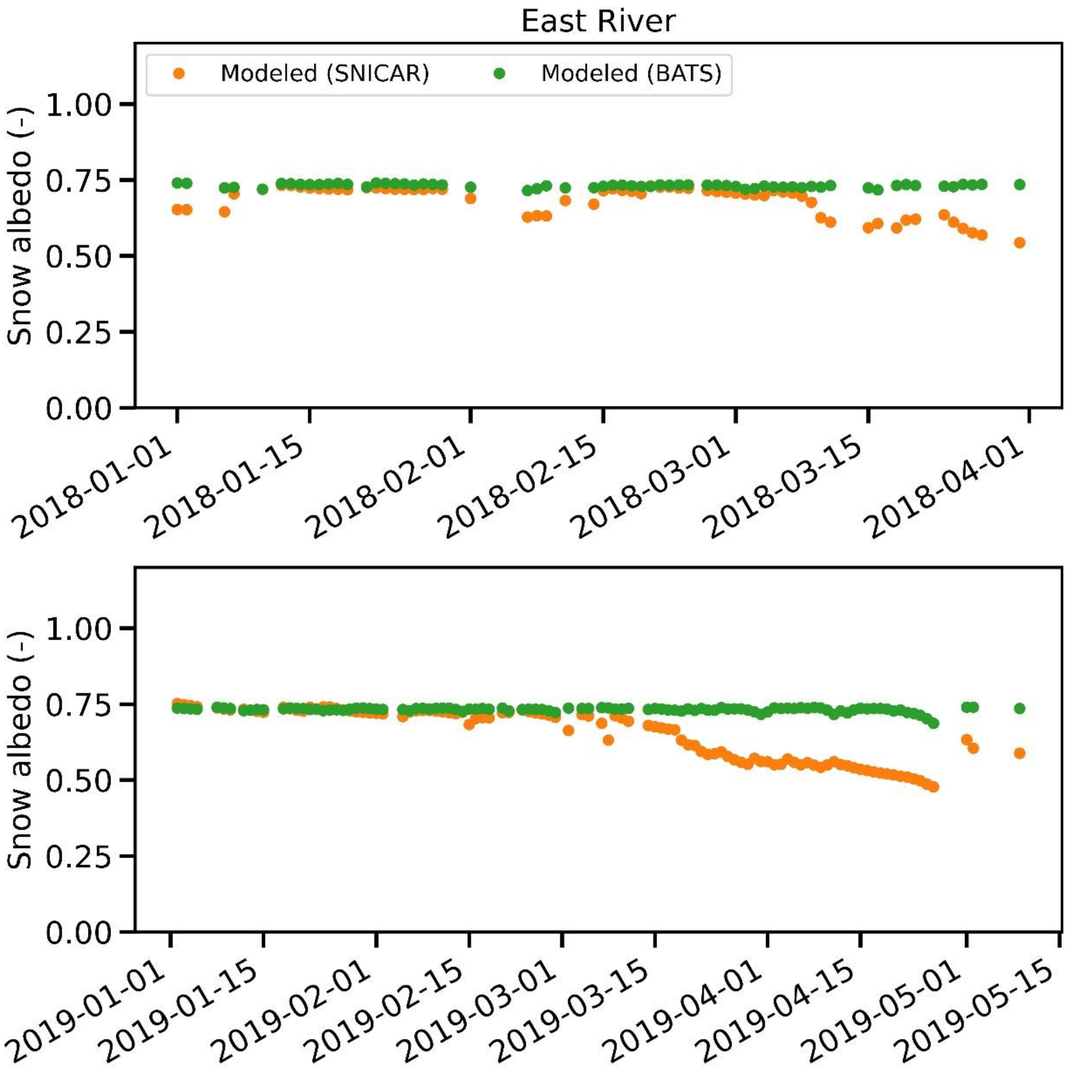

Fig. S5c. Similar to Fig. S3c but in near-infrared wavelengths.

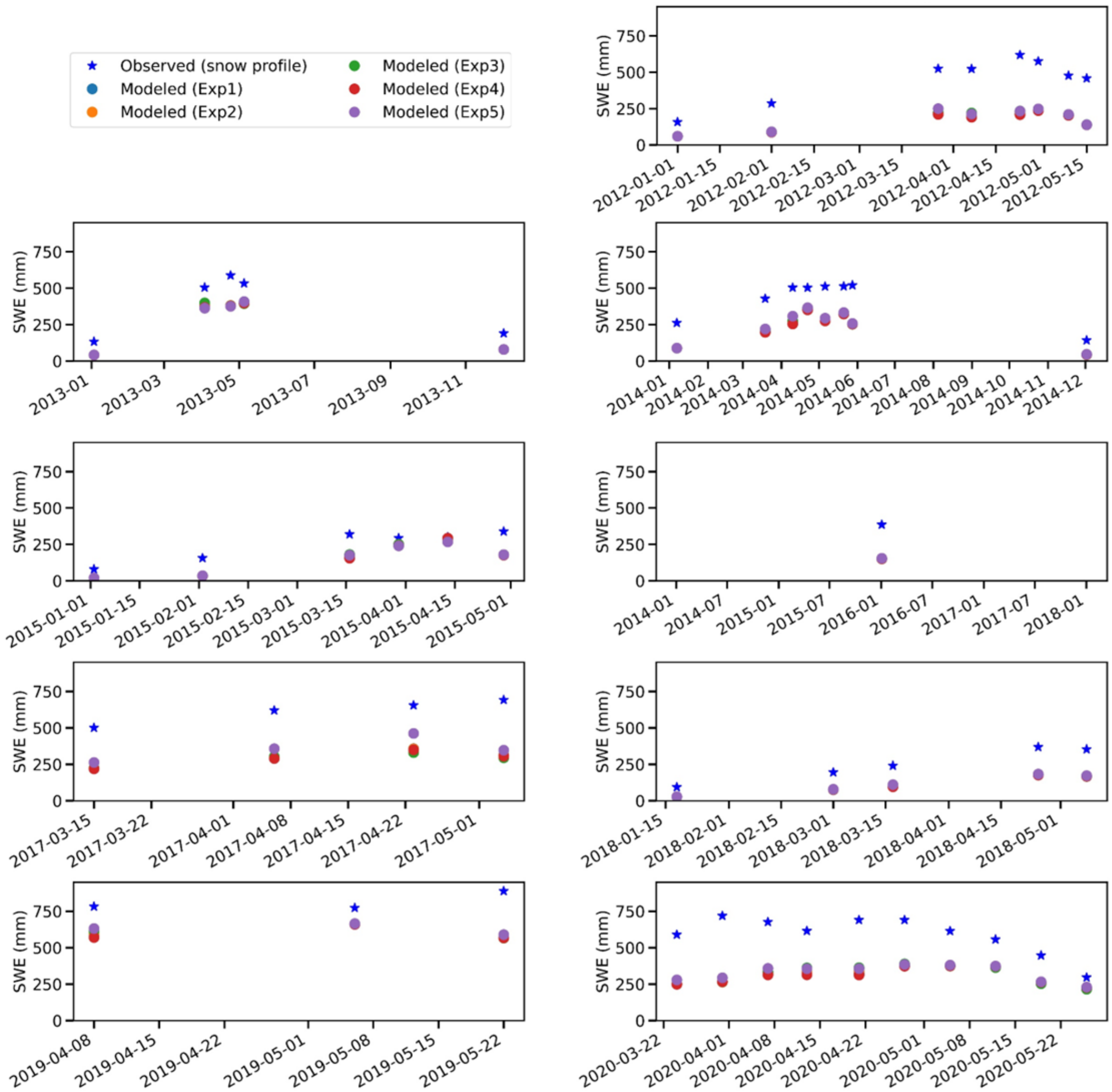

Fig. S6. Comparison of snow water equivalent (SWE) between measurements from snow profiles (blue stars) and Noah-MP simulations of different model experiments (Table 1) at the Senator Beck station.

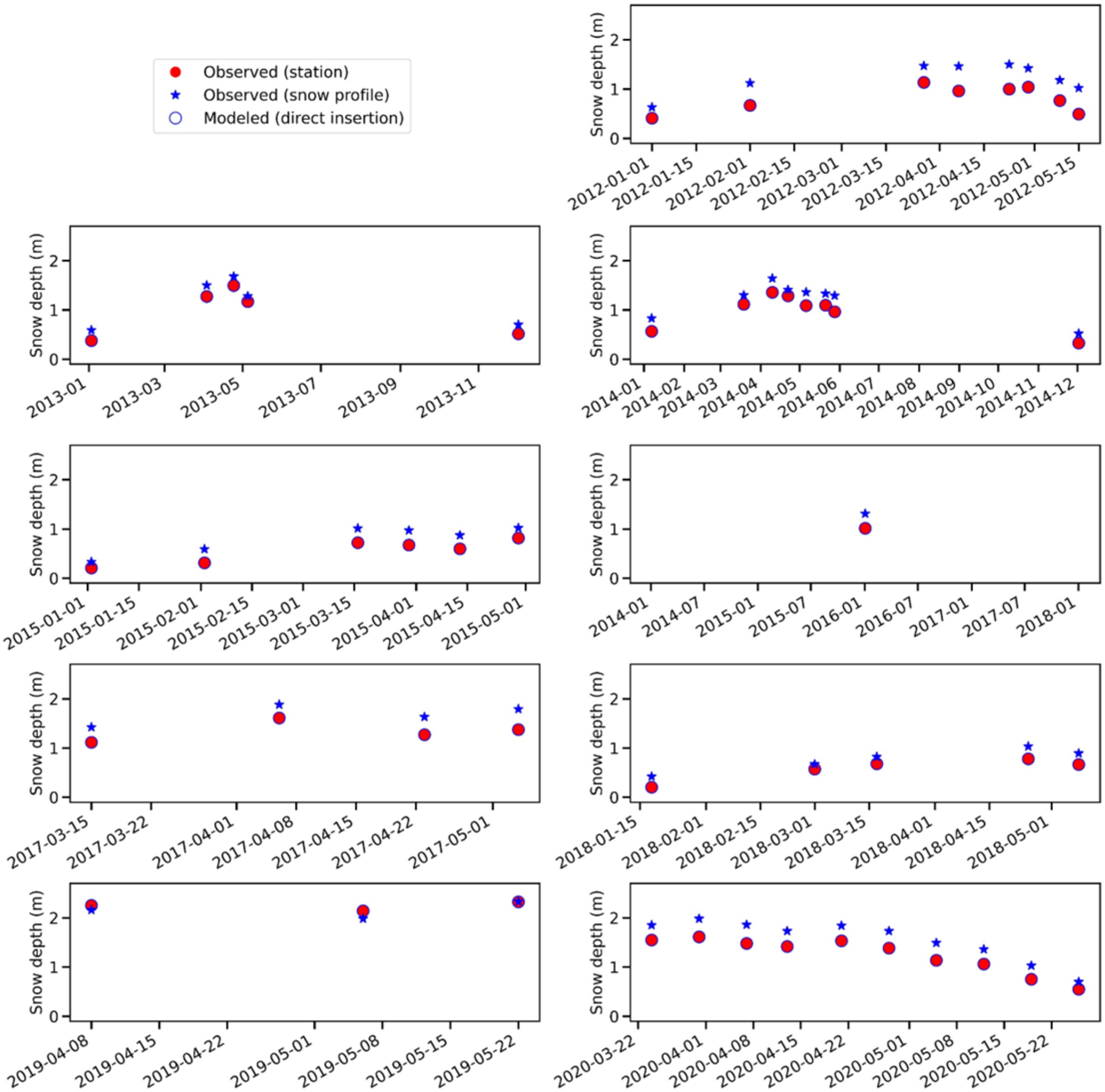

Fig. S7. Comparison of observed snow depth at the Senator Beck site. Red circles represent measurements from the automated station, blue stars represent measurements from snow profiles, and blue circles represent Noah-MP simulated snow depth from direct insertion.

Table S1. Information of three in-situ observational sites.

Site name	Elevation (m)	Latitude	Longitude	Albedo spectrum bands	Vegetation types	Observed climate variables	Model spin up period	Analysis period
Irwin	3168	38.8872°	-107.1084°	NIR, VIS, and broadband	sparse forest canopy and grass understory	Temperature and downward shortwave radiation	13 years (1 October 2015 to 30 September 2016, 10 times in series; then 1 October 2015 to September 2018)	October 2018 to August 2021
Senator Beck	3714	37.9069°	-107.7263°	NIR, VIS, and broadband	tundra	Temperature, downward shortwave radiation, downward longwave radiation, precipitation, wind speed, pressure, and specific humidity	11 years (1 October 2010 to 30 September 2019 then 1 October 2010 to 30 September 2011)	October 2011 to 2020 October
East River	2762	38.9224°	-106.9497°	Broadband	riparian grasses and willow galleries	Temperature, downward longwave radiation, and downward shortwave radiation	13 years (1 October 2015 to 30 September 2016, 10 times in series; then 1 October 2015 to 1 June 2017)	July 2017 to November 2019

Table S2. Conversion of the dust aerosol size (μm in diameter) used in MERRA-2 to Noah-MP/SNICAR. The values represent mass fraction of dust deposition from MERRA-2 into each size bin of dust in snow in Noah-MP/SNICAR.

MERRA-2 dust size bin	Noah-MP/SNICAR dust size bin				
	0.1-1.0 μm	1.0-2.5 μm	2.5-5.0 μm	5.0-10.0 μm	10.0-100.0 μm
0.2-2.0 μm	0.44	0.56	0	0	0
2.0-3.6 μm	0	0.31	0.69	0	0
3.6-6.0 μm	0	0	0.58	0.42	0
6.0-12.0 μm	0	0	0	0.67	0.33
12.0-20.0 μm	0	0	0	0	1

Table S3. Observed and modeled mean, median, and interquartile range of snow albedo for three sites. Numbers in square brackets are the first quartile, median, and third quartile, respectively.

	Broadband			Visible			Near-infrared		
	All	**Fresh**	**Melt**	**All**	**Fresh**	**Melt**	**All**	**Fresh**	**Melt**
Senator Beck									
Observed	0.77 [0.74;0.79;0.83]	0.87 [0.85;0.88;0.89]	0.68 [0.58;0.69;0.79]	0.87 [0.85;0.89;0.93]	0.93 [0.93;0.94;0.95]	0.81 [0.72;0.86;0.91]	0.67 [0.63;0.70;0.75]	0.79 [0.77;0.79;0.82]	0.56 [0.44;0.53;0.67]
Modeled (SNICAR)	0.83 [0.81;0.85;0.87]	0.86 [0.85;0.87;0.89]	0.78 [0.75;0.79;0.83]	0.95 [0.94;0.97;0.98]	0.97 [0.96;0.97;0.98]	0.93 [0.93;0.95;0.96]	0.71 [0.66;0.73;0.78]	0.76 [0.73;0.77;0.80]	0.63 [0.56;0.63;0.68]
Modeled (BATS)	0.82 [0.82;0.82;0.82]	0.82 [0.82;0.82;0.83]	0.81 [0.81;0.82;0.82]	0.90 [0.91;0.91;0.91]	0.91 [0.91;0.91;0.91]	0.89 [0.91;0.91;0.91]	0.73 [0.73;0.74;0.74]	0.74 [0.73;0.74;0.74]	0.72 [0.73;0.73;0.74]
Irwin									
Observed	0.71 [0.62;0.75;0.81]	0.82 [0.79;0.84;0.85]	0.60 [0.52;0.60;0.68]	0.82 [0.76;0.87;0.91]	0.90 [0.89;0.90;0.92]	0.73 [0.64;0.76;0.85]	0.59 [0.44;0.63;0.70]	0.72 [0.67;0.73;0.79]	0.46 [0.39;0.43;0.51]
Modeled (SNICAR)	0.77 [0.72;0.79;0.83]	0.82 [0.79;0.82;0.84]	0.70 [0.68;0.71;0.74]	0.90 [0.88;0.93;0.96]	0.93 [0.92;0.93;0.96]	0.85 [0.82;0.87;0.91]	0.61 [0.53;0.63;0.68]	0.69 [0.65;0.68;0.72]	0.52 [0.50;0.52;0.55]
Modeled (BATS)	0.82 [0.82;0.82;0.83]	0.83 [0.82;0.82;0.83]	0.80 [0.81;0.82;0.83]	0.89 [0.90;0.91;0.91]	0.91 [0.91;0.91;0.91]	0.87 [0.89;0.91;0.91]	0.72 [0.73;0.73;0.74]	0.73 [0.73;0.74;0.74]	0.71 [0.72;0.73;0.74]
East River									
Observed	0.71 [0.62;0.71;0.79]	0.76 [0.64;0.76;0.86]	0.66 [0.61;0.66;0.70]						
Modeled (SNICAR)	0.80 [0.76;0.83;0.85]	0.82 [0.81;0.83;0.85]	0.76 [0.71;0.77;0.84]	0.93 [0.92;0.96;0.97]	0.95 [0.92;0.95;0.97]	0.91 [0.86;0.93;0.97]	0.66 [0.59;0.70;0.72]	0.70 [0.70;0.72;0.72]	0.62 [0.55;0.61;0.71]
Modeled (BATS)	0.82 [0.82;0.82;0.82]	0.82 [0.82;0.82;0.82]	0.82 [0.82;0.82;0.82]	0.90 [0.91;0.91;0.91]	0.91 [0.91;0.91;0.91]	0.90 [0.90;0.91;0.91]	0.73 [0.73;0.73;0.74]	0.73 [0.73;0.73;0.74]	0.73 [0.73;0.73;0.73]

Table S4a. The modeled broadband snow albedo bias, root mean square error (RMSE), and correlation coefficient (r) with measurements over study periods for three sites (Senator Beck, Irwin, and East River).

Modeled albedo scheme	Modeled snow depth	Bias	RMSE	r
SNICAR	direct insertion	0.065	0.103	0.67
BATS	direct insertion	0.062	0.116	0.42
SNICAR	open-loop	-0.061	0.166	0.69
BATS	open-loop	-0.049	0.134	0.72

Table S4b. Similar to Table S4a but in visible wavelengths for two sites (Senator Beck and Irwin).

Modeled albedo scheme	Modeled snow depth	Bias	RMSE	r
SNICAR	direct insertion	0.084	0.115	0.59
BATS	direct insertion	0.039	0.094	0.49
SNICAR	open-loop	-0.103	0.241	0.62
BATS	open-loop	-0.082	0.200	0.68

Table S4c. Similar to Table S4a but in near-infrared wavelengths for two sites (Senator Beck and Irwin).

Modeled albedo scheme	Modeled snow depth	Bias	RMSE	r
SNICAR	direct insertion	0.034	0.091	0.74
BATS	direct insertion	0.073	0.138	0.40
SNICAR	open-loop	-0.023	0.109	0.72
BATS	open-loop	-0.038	0.095	0.78

Table S5a. Model simulated mean changes in snow albedo due to changes in snow grain size from original fresh snow grain parameters to optimized ones, snow grain shape from sphere to hexagonal shape, and light-absorbing particles (LAPs) from no LAPs to with LAPs in three stations.

	Broadband			Visible			Near-infrared		
	All	**Fresh**	**Melt**	**All**	**Fresh**	**Melt**	**All**	**Fresh**	**Melt**
Senator Beck									
Grain size	0.022	0.030	0.010	0.011	0.014	0.005	0.034	0.047	0.016
Grain shape	0.037	0.030	0.043	0.021	0.016	0.027	0.054	0.046	0.061
LAPs	-0.012	-0.010	-0.017	-0.019	-0.016	-0.028	-0.005	-0.003	-0.005
Irwin									
Grain size	0.011	0.023	0.003	0.006	0.012	0.002	0.017	0.036	0.004
Grain shape	0.042	0.036	0.050	0.031	0.022	0.046	0.054	0.053	0.056
LAPs	-0.031	-0.029	-0.046	-0.053	-0.048	-0.079	-0.005	-0.003	-0.004
East River									
Grain size	0.021	0.028	0.016	0.010	0.014	0.008	0.033	0.042	0.023
Grain shape	0.039	0.034	0.044	0.022	0.018	0.027	0.056	0.050	0.061
LAPs	-0.024	-0.020	-0.033	-0.042	-0.036	-0.060	-0.006	-0.005	-0.007

Table S5b. Similar to Table S5a but for induced surface radiative forcing (W/m^2).

	Broadband			Visible			Near-infrared		
	All	**Fresh**	**Melt**	**All**	**Fresh**	**Melt**	**All**	**Fresh**	**Melt**
Senator Beck									
Grain size	-14.15	-16.09	-9.11	-3.50	-3.79	-2.11	-10.65	-12.30	-6.99
Grain shape	-26.87	-17.17	-39.07	-7.90	-4.61	-12.53	-18.96	-12.56	-26.54
LAPs	8.74	5.66	14.85	7.04	4.85	12.53	1.69	0.82	2.31
Irwin									
Grain size	-6.10	-8.75	-2.32	-1.84	-2.67	-0.83	-4.26	-6.08	-1.49
Grain shape	-29.48	-14.83	-43.3	-12.77	-5.29	-21.55	-16.72	-9.54	-21.75
LAPs	22.23	12.84	36.65	20.77	12.31	35.04	1.46	0.52	1.62
East River									
Grain size	-12.89	-12.15	-10.52	-2.95	-3.00	-2.64	-9.94	-9.15	-7.88
Grain shape	-26.18	-16.36	-32.95	-7.40	-4.33	-10.17	-18.77	-12.03	-22.77
LAPs	16.68	9.27	25.27	14.68	7.96	22.63	2.00	1.31	2.64

Table S6. The comparison of dust deposition (g/m^2) from MERRA-2 used in Noah-MP simulations at Senator Beck site for water year 2012-2016 with mass loading data (https://www.codos.org/#mass-loading-data, Reynolds et al. 2020) at Swamp Angel Study Plot.

Water Year	MERRA-2	Mass loading data
2012	0.64	7.07
2013	0.88	50.11
2014	0.88	30.86
2015	0.82	5.62
2016	0.67	9.57